Supporting Information

Bismuthene from Sonoelectrochemistry as Superior Anode for Potassium-Ion Batteries

Chao Shen, [a] Tianle Cheng, [a] Chunyan Liu,[a] Lu Huang, *[a] Mengyang Cao, [a] Ganqiang Song, [a] Dong Wang, [a] Bingan Lu, [b] Jianwen Wang, [a] Chichu Qin, [a] Xingkang Huang, [c] Ping Peng, [d] Xilong Li, [a] Yingpeng Wu*[a]

[a] State Key Laboratory of Chem/Bio-Sensing and Chemometrics, Provincial Hunan Key Laboratory for Graphene Materials and Devices, College of Chemistry and Chemical Engineering, Hunan University, Changsha, 410082, P. R. China.

E-mail: luhuang@hnu.edu.cn, wuyingpeng@hnu.edu.cn

[b] College of physics and Electronics, Hunan University, Changsha 410082, PR China

[c] Department of Mechanical Engineering, College of Engineering & Applied Sciences, University of Wisconsin-Milwaukee, 3200 North Cramer Street, Milwaukee, WI, 53211, USA

[d] College of Material and Engineering, Hunan University, Changsha 410082, PR China

Table S1. Countrol experiments for the exfoliation process: with different operating voltages, with/without ultrasonication and with/without potassium hydroxide.

Number	Voltage[v]	Ultrasound	KOH	Remarks
1	5	Yes	Yes	Figure S1-a_1
2	5	Yes	/	Figure S1-a_2
3	5	/	Yes	Figure S1-a_3
4	5	/	/	Figure S1-a_4
5	10	Yes	Yes	Figure S1-b_1
6	10	Yes	/	Figure S1-b_2
7	10	/	Yes	Figure S1-b_3
8	10	/	/	Figure S1-b_4
9	15	Yes	Yes	Figure S1-c_1
10	15	Yes	/	Figure S1-c_2
11	15	/	Yes	Figure S1-c_3
12	15	/	/	Figure S1-c_4
13	20	Yes	Yes	Figure S1-d_1
14	20	Yes	/	Figure S1-d_2
15	20	/	Yes	Figure S1-d_3
16	20	/	/	Figure S1-d_4

Table S1 listed the detailed information of the exfoliation process under different conditions. The corresponding cross-sectional SEM images of those products were shown in Figure S1. With the increase of the operated voltage, the size of final products was decreasing. At voltage of 15 V, bismuth nanosheets can be observed in Figure S1-c_1. With the dual assistance of ultrasound and KOH additive, uniform and stable bismuthene nanosheets were obtained at the optimal condition (Number 9).

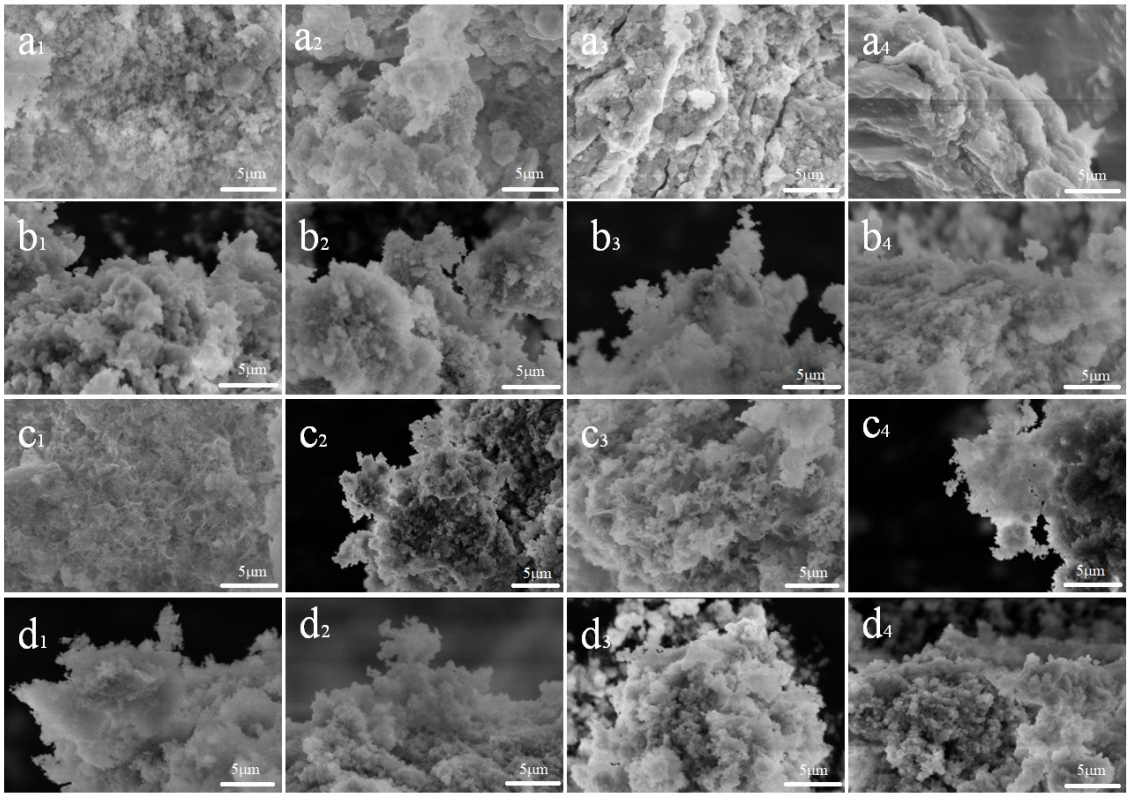

Figure S1. SEM images at different preparation conditions. A_1-a_4 were got at the voltage of 5 V; b_1-b_4 were at the voltage of 10 V; c_1-c_4 were at the voltage of 15 V; d_1-d_4 were at the voltage of 20 V.

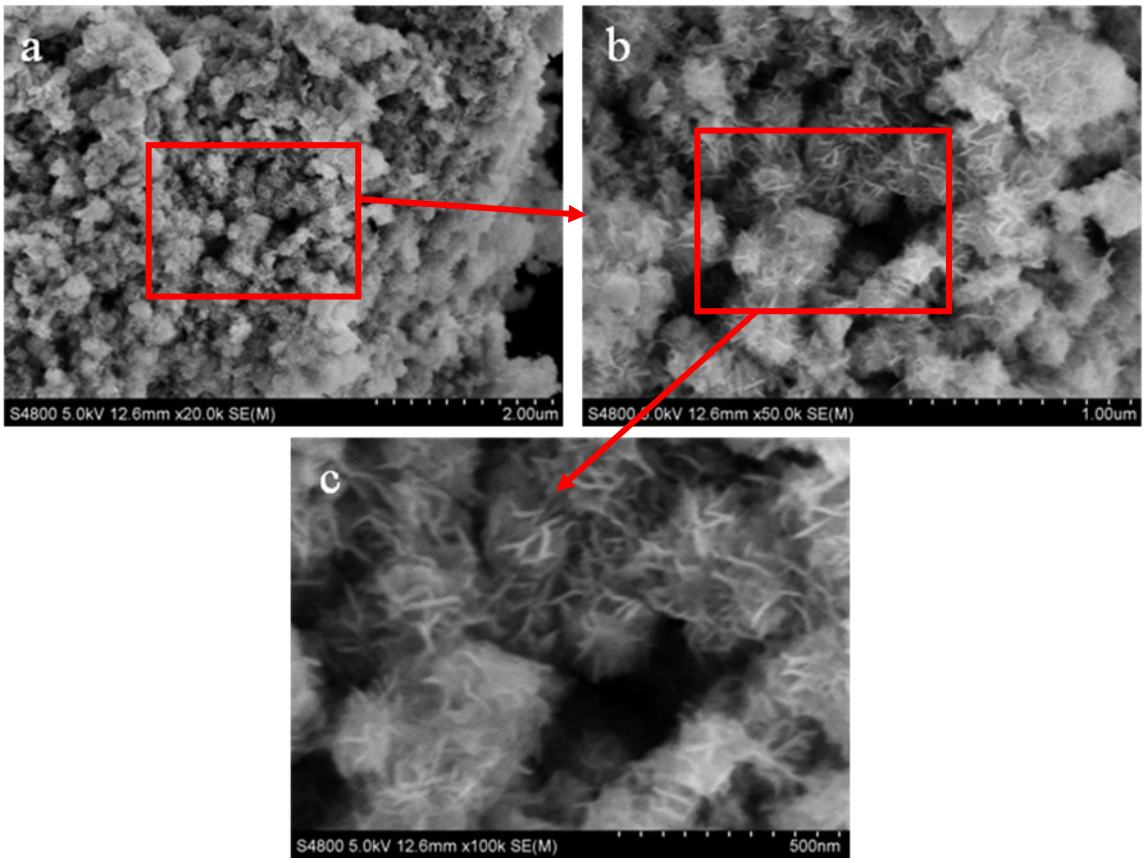

Figure S2. SEM images of FBNs at different magnification

Figure S2-b was the magnified picture of the red circle in Figure S2-a and Figure S2-c was the magnified picture of the red circle in Figure S2-b. These SEM images clearly revealed the few-layered bismuthene nanosheets with ultrathin 2D structure. Such structure could contribute to excellent electrochemical behaviours in KIBs as the anode.

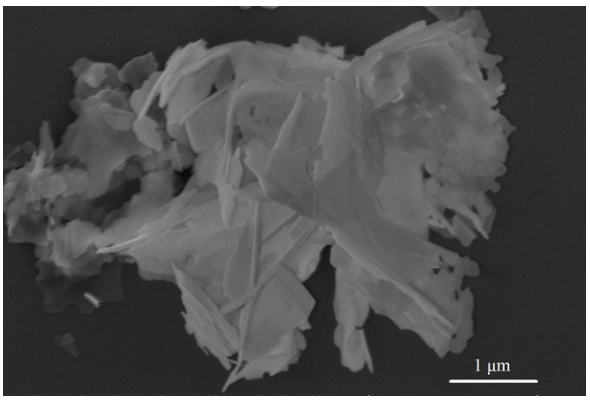

Figure S3. High resolution SEM images of FBNs.

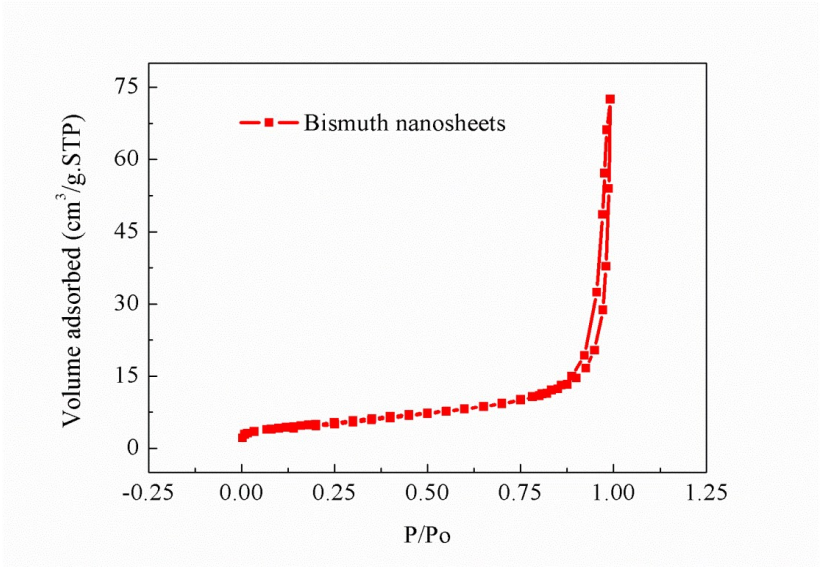

Figure S4. BET measurement curve of FBNs

The Brunauer-Emmett-Teller (BET) surface area of FBNs was 18 m^2/g. The large surface area agreed with the TEM and AFM results which indicated the FBNs were successful obtained.

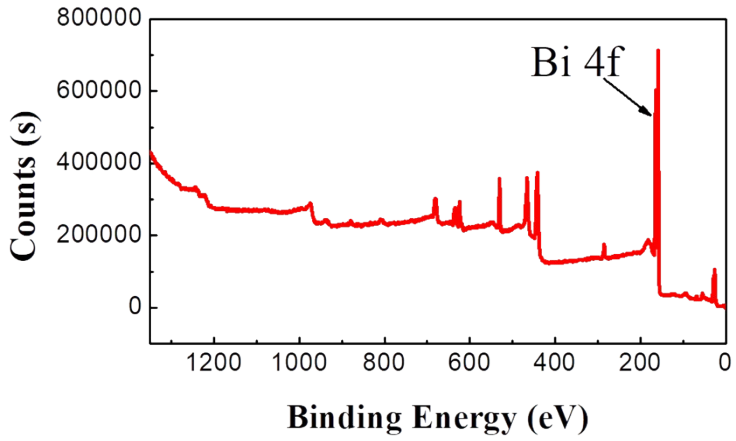

Figure S5. XPS analysis of FBNs

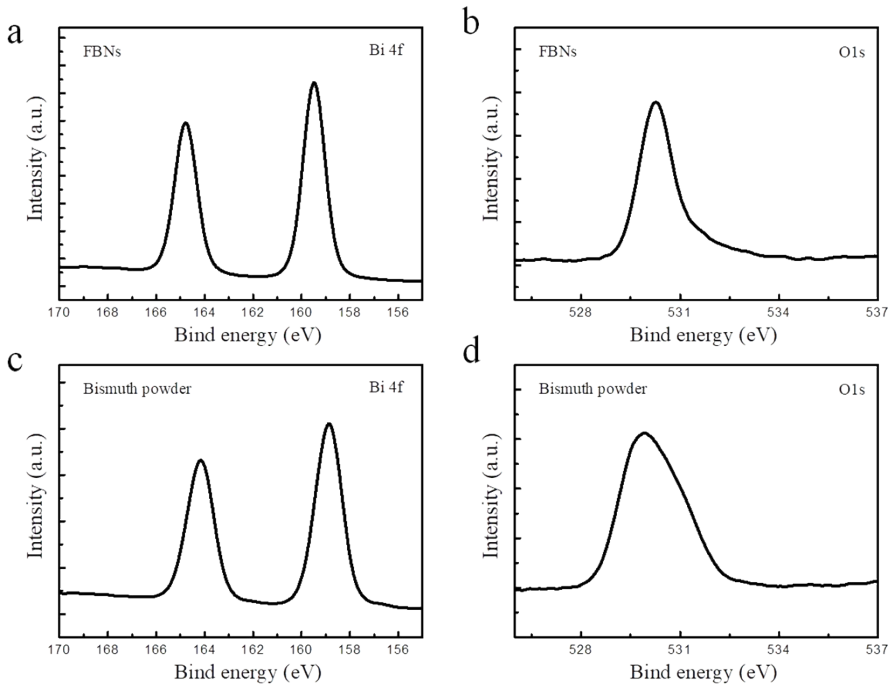

Figure S6. a,b are the XPS spectra of Bi and O of FBNs; c,d are the XPS spectra of Bi and O of bismuth powder.

From the consequence of high solution XPS spectra of Bi and O, the additional signal may be derived from the adsorbed O_2 on the surface of FBNs, the binding energies located at 159.3 and 164.8 eV is corresponding to Bi $4f_{5/2}$ and Bi $4f_{7/2}$. To compare the extent of oxide for FBNs, we test the bismuth powder simultaneously. The peak of Bi and O are nearly consistent between FBNs and bulk bismuth powder.

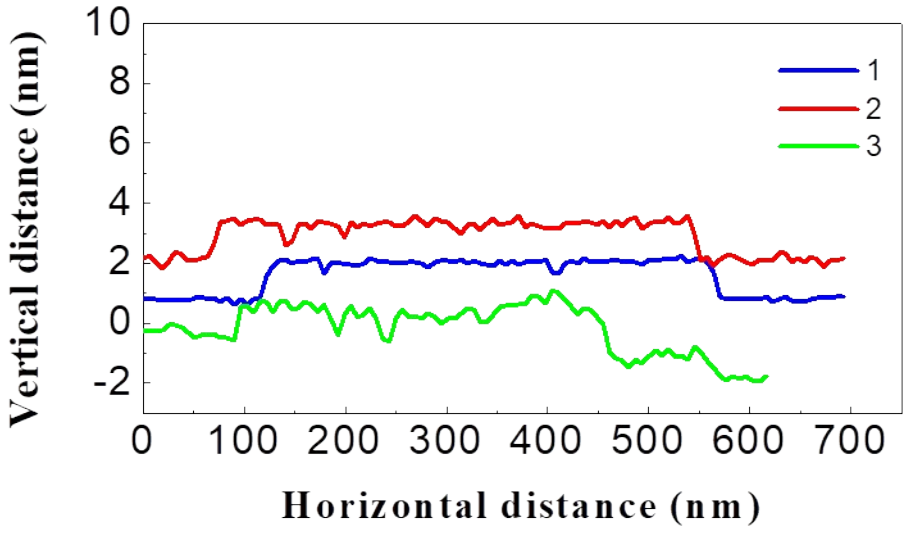

Figure S7. AFM analysis of FBNs

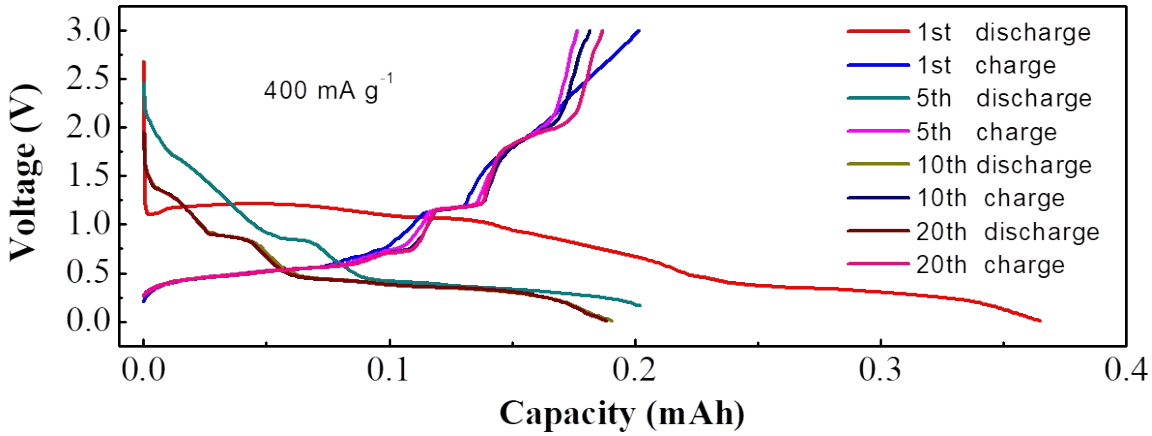

Figure S8. Galvanostatic charge and discharge curves of FBNs at current density of 400 mA g^{-1}

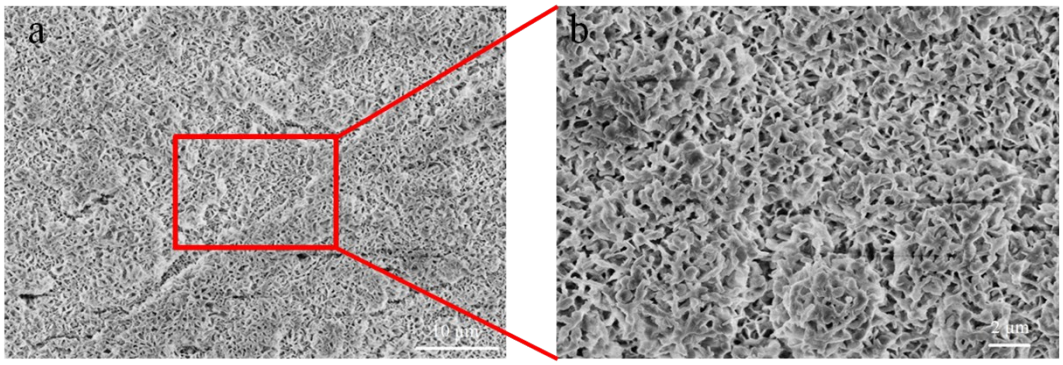

Figure S9. The morphology of the FBNs electrode after cycles at different magnification.

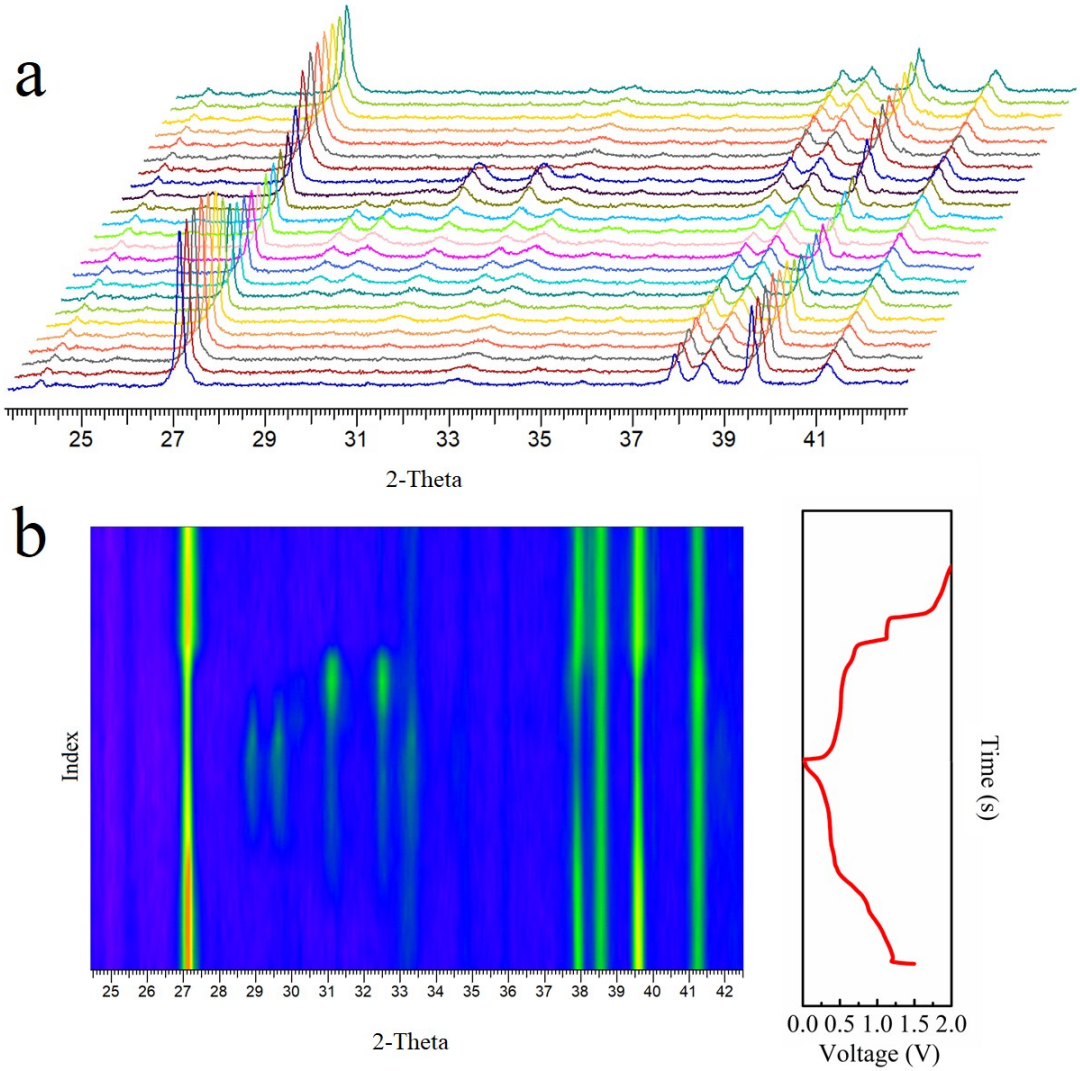

Figure S10. Operando XRD of FBNs anode at a current density of 100 mA g^{-1}. a) The XRD patterns during the initial discharge-charge. b) Contour plot of in-situ XRD measurement of FBNs. On the right hand side, the corresponding galvanostatic curve was shown.

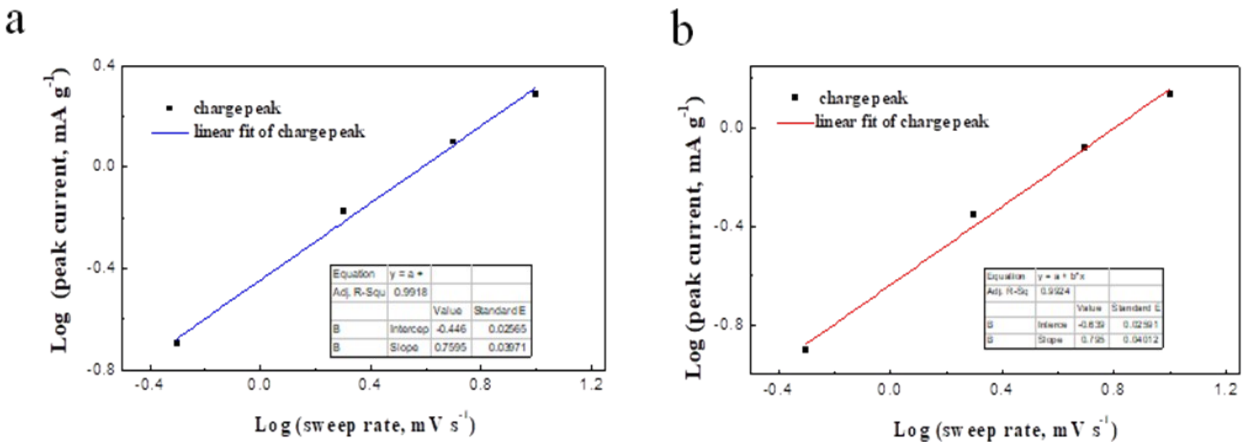

Figure S11: Kinetics analysis of the electrochemical behavior for FBNs. a,b) b value of 0.759 and 0.795 were calculated from the discharge peak and charge peak, respectively.

Table S2. Parameter values obtained from the EIS data fitting of FBNs anode.

Par	Value	Error/%	Min	Max	Unit
R_s	3.061×10^{1}	0.97	1.0×10^{-4}	1.0×10^{13}	Ohm
R_f	2.531×10^{2}	5.09	1.0×10^{-4}	1.0×10^{13}	Ohm
R_{ct}	5.208×10^{0}	6.48	1.0×10^{-4}	1.0×10^{13}	Ohm
C_1	6.55×10^{-4}	2.45	1.0×10^{-13}	1.0×10^{1}	F
C_2	1.106×10^{-5}	14.19	1.0×10^{-13}	1.0×10^{1}	F
Z_w	5.661×10^{-3}	13.82	1.0×10^{-12}	1.0×10^{6}	1/(Ohm sqr)

Table S3. Parameter values obtained from the EIS data fitting of Bismuth powder anode.

Par	Value	Error/%	Min	Max	Unit
R_s	2.782×10^{1}	13.15	1.0×10^{-4}	1.0×10^{13}	Ohm
R_f	1.395×10^{2}	5.37	1.0×10^{-4}	1.0×10^{13}	Ohm
R_{ct}	2.222×10^{2}	3.27	1.0×10^{-4}	1.0×10^{13}	Ohm
C_1	9.895×10^{-6}	9.72	1.0×10^{-13}	1.0×10^{1}	F
C_2	1.213×10^{-4}	8.42	1.0×10^{-13}	1.0×10^{1}	F
Z_w	4.276×10^{-3}	2.20	1.0×10^{-12}	1.0×10^{6}	1/(Ohm sqr)

Table S2 and S3 showed the fitting parameter values of FBNs and bismuth power as the anode. R_f was related to the resistance of contact. R_{ct} signified the charge transfer. R_{ct} values indicated that the FBNs possessed a faster charge transfer capacity than the bismuth power.

Table S4. Comparison of anode performance between literature and our current work

Anode material	Initialcapacity (depotassiation) [mAh g^{-1}]	1st CE[%]	current density [mAg^{-1}]	Cycle number	Ref.
Bi	397.8	80.2	(2C) 795.6	300	[1]
Sb nanoparticles in 3D porous carbon	596.8	46.2	100	100	[2]
CoS@graphene	434.5	64.4	(0.5C) 217.25	100	[3]
Bi/rGO	441	63	50	50	[4]
Black phosphorus/C (B:C = 1:1)	433.2	58.5	50	50	[5]
Nitrogen-doped graphene	330	80	100	50	[6]
Graphite	279	87	25	50	[7]
Hard carbon microspheres	≈270	≈62	(0.1C) 27	100	[8]
Hard carbon–derived from tire rubber	181	33	(0.5C) 90.5	200	[9]
MoS2	98	74.4		200	[10]

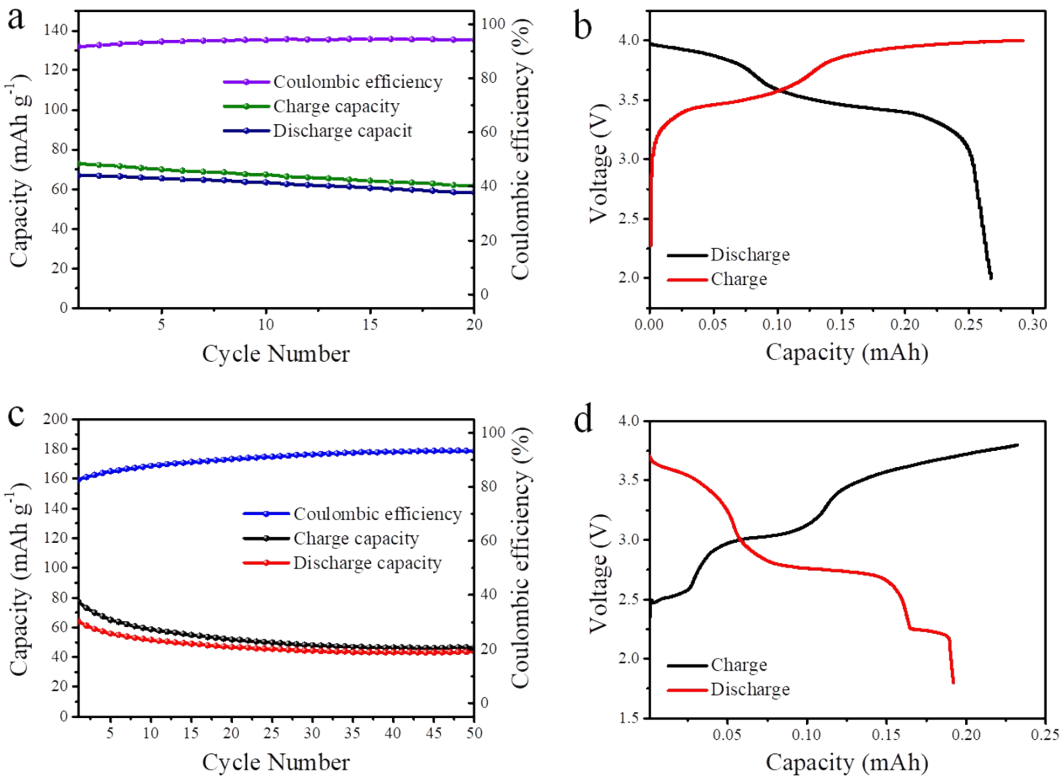

Figure S12. (a) and (b) are Electrochemical performance of the cathode PB in the voltage range of 2-4 V at 200 mAh g^{-1} Cycling performance and charge-discharge curves. (c) and (d) are Electrochemical performance of the full cell in the voltage range of 1.8-3.8 V at 200 mAh g^{-1} Cycling performance and charge-discharge curves.

The preparation of full battery:

1: Prussian blue was prepared as follows. Firstly, 2.0 mmol of $K_4Fe(CN)_6$ and 4.0 mmol of $FeCl_3$ were separately dissolved in 160.0 and 40.0 mL of deionized water. Then, the $FeCl_3$ solution was dropwise added into the $K_4Fe(CN)_6$ solution. After stirring for 2 h, the mixture was aged for 24 h at room temperature. The obtained dark blue precipitates were centrifuged, washed by water and alcohol for several times, and dried at 80°C in a vacuum oven for 24 h finally.

2: The obtained Prussian blue, conductive agent (acetylene black), and 0.6% PTFE water solution with a mass ratio of 8:1:1 in alcohol solution were ultrasonic dispersion and dry over 12 h at 80°C in a vacuum oven. Then, the dried active material was rolled into electrode slice.

3: Prussian blue electrode slice and the potassium foil was assembled into half-cell and 1 M KPF_6 in DME was used as the electrolyte. Whatman GF/D glass fiber paper was utilized as separator. Then, Prussian blue with full embedding potassium was obtained by discharging the half cell to 2.0 V. Finally, the FBNs electrode and Prussian blue with full embedding potassium were assembled into full cell with capacity ratio at 1.05:1.

As show in Figure S12, we had assembled full cells and achieved a large energy density of 127 Wh kg^{-1} with average discharge voltage of 2.8V.

References

1. K. Lei, C. Wang, L. Liu, Y. Luo, C. Mu, F. Li, J. Chen, *Angew. Chem. Int. Ed. Engl.* **2018**, *57*, 4687-4691.

2. H. Wang, X. Wu, X. J. Qi, W. Zhao, Z. C. Ju, Mater. Res. Bull. 2018, **103**, 32-37.

3. H. Gao, T. F. Zhou, Y. Zheng, Q. Zhang, Y. Q. Liu, J. Chen, H. K. Liu, Z. P. Guo, Adv. Funct. Mater. 2017, **27**. 1702634-1702642.

4. Q. Zhang, J. Mao, W. K. Pang, T. Zheng, V. Sencadas, Y. Chen, Y. Liu, Z. Guo, Adv. Energy Mater. 2018, **8**, 1703288.

5. I. Sultana, M. M. Rahman, T. Ramireddy, Y. Chen, A. M. Glushenkov, J. Mater. Chem. A 2019, **7**, 2421-2421.

6. J. Zhi, S. Li, M. Han, Y. Lou, P. Chen, Adv. Energy Mater. 2018, **8**, 1802254.

7. S. Komaba, T. Hasegawa, M. Dahbi, K. Kubota, Electrochem. Commun. 2015, **60**, 172-175.

8. Z. Jian, Z. Xing, C. Bommier, Z. Li, X. Ji, Adv. Energy Mater. 2016, **6**, 1501874.

9. Y. C. Li, R. A. Adams, A. Arora, V. G. Pol, A. M. Levine, R. J. Lee, K. Akato, A. K. Naskar, M. P. Paranthaman, J. Electrochem. Soc. 2017, **164**, A1234-A1238.

10. X. Ren, Q. Zhao, W. D. McCulloch, Y. Wu, Nano Research 2017, **10**, 1313-1321.